# A high-fat diet suppresses de novo lipogenesis and desaturation but not elongation and triglyceride synthesis in mice[S]

**Joao A. G. Duarte,*,† Filipa Carvalho,† Mackenzie Pearson,* Jay D. Horton,§ Jeffrey D. Browning,*,§ John G. Jones,† and Shawn C. Burgess[1],*,****

Advanced Imaging Research Center-Division of Metabolic Mechanisms of Disease,* Department of Internal Medicine,§ and Department of Pharmacology,** The University of Texas Southwestern Medical Center, Dallas, TX; and Center for Neurosciences and Cell Biology, Department of Zoology,† University of Coimbra, Coimbra, Portugal

**Abstract Intracellular lipids and their synthesis contribute to the mechanisms and complications of obesity-associated diseases. We describe an NMR approach that provides an abbreviated lipidomic analysis with concurrent lipid biosynthetic fluxes. Following deuterated water administration, positional isotopomer analysis by deuterium NMR of specific lipid species was used to examine flux through de novo lipogenesis (DNL), FA elongation, desaturation, and TG-glycerol synthesis. The NMR method obviated certain assumptions regarding sites of enrichment and exchangeable hydrogens required by mass isotope methods. The approach was responsive to genetic and pharmacological gain or loss of function of DNL, elongation, desaturation, and glyceride synthesis. BDF1 mice consuming a high-fat diet (HFD) or matched low-fat diet for 35 weeks were examined across feeding periods to determine how flux through these pathways contributes to diet induced fatty liver and obesity. HFD mice had increased rates of FA elongation and glyceride synthesis. However DNL was markedly suppressed despite insulin resistance and obesity.[FLR] We conclude that most hepatic TGs in the liver of HFD mice were formed from the reesterification of existing or ingested lipids, not DNL.**—Duarte, J. A. G., F. Carvalho, M. Pearson, J. D. Horton, J. D. Browning, J. G. Jones, and S. C. Burgess. **A high-fat diet suppresses de novo lipogenesis and desaturation but not elongation and triglyceride synthesis in mice. *J. Lipid Res.* 2014.** 55: **2541–2553.**

**Supplementary key words** lipid metabolism • obesity • liver • adipose • nuclear magnetic resonance • lipidomics

Lipid metabolism is dysregulated in many diseases, including obesity and diabetes. During obesity, ectopic lipids trigger oxidative stress, inflammation, and cell-signaling events that disrupt insulin action and lead to type 2 diabetes (1, 2). Despite insulin resistance, insulin continues to induce sterol-regulatory element binding protein 1 (SREBP-1)-mediated lipogenic genes in liver (3–5). Nonalcoholic fatty liver disease (NAFLD) is associated with obesity/insulin resistance in humans and is due in part to this elevated de novo lipogenesis (DNL) (6). However, studies in lipogenic flux in obese and insulin-resistant rodent models consuming a high-fat diet (HFD) have found increased (7), no change (8), and decreased lipogenesis (9–11). In this sense, the functional role of lipogenesis is less clear than the molecular events that alter lipogenic gene expression in diet-induced obesity and insulin resistance.

In addition to DNL, the elongation and desaturation of lipids also have important implications for obesity and insulin resistance (12). DHA and other long-chain PUFAs are formed by elongation of very long chain fatty acids (ELOVL)-mediated elongation of essential FAs (13). Some of these lipids beneficially activate PPAR pathways, such as lipid oxidation and storage, and repress SREBP-1-mediated lipogenesis (14). Others form eicosanoids, which interact with inflammatory pathways that mediate the transition from benign NAFLD to steatohepatitis (15). In contrast, endogenous desaturation of lipids by sterol-CoA desaturase 1 (SCD-1) to monounsaturated fats (16) and/or elongation of these lipids may promote (17) or protect against NAFLD (12) and its progression to steatohepatitis. Thus,

*Support for this work was provided by National Institutes of Health Grants DK078184 (S.C.B.), DK058398 (S.C.B.), HL020948 (J.D.H), DK087977 (J.D.B), and EB015908 (Center resources), and by the Robert A. Welch Foundation (S.C.B.). J.A.G.D and J.G.J were supported by Portuguese Foundation for Science and Technology grants SFRH/BD/44294/2008 and PTDC/SAU-MET/111398/2009.*

*Manuscript received 24 June 2014 and in revised form 29 September 2014.*

*Published, JLR Papers in Press, September 30, 2014*
*DOI 10.1194/jlr.M052308*

Abbreviations: AMW, average molecular weight; ANC, average number of carbons; ANP, average number of protons; DNL, de novo lipogenesis; ELOVL, elongation of very long chain fatty acids; HFD, high-fat diet; LFD, low-fat diet; MIDA, mass isotopomer distribution analysis; NAFLD, nonalcoholic fatty liver disease; PABA, para-amino benzoic acid; SCD-1, sterol-CoA desaturase 1; SREBP-1, sterol-regulatory element binding protein 1; WAT, white adipose tissue.

[1]To whom correspondence should be addressed.
e-mail: shawn.burgess@utsouthwestern.edu

[S] The online version of this article (available at http://www.jlr.org) contains supplementary data in the form of eight tables and one figure.

examination of these species, in addition to DNL, is likely important in the context of disease.

The importance of lipid metabolism in physiology and disease stimulated the development of modern lipidomic methods. Large libraries of lipid species have been evaluated by MS-linked databases (18), providing associations between lipid profiles and physiology. Isotope tracers that incorporate into lipids during synthesis have been used to measure intracellular lipid flux, providing mechanistic insight into the regulation of these pathways. In principal, mass enrichment of $^{13}C$ or $^{2}H$ tracers can be detected in any newly synthesized lipid using MS and chromatographic separation (19). One common approach uses $^{2}H$ enrichment in tissue or plasma TG palmitate following $^{2}H_2O$ administration to examine DNL (20). Longer-chain FAs and the glyceride moiety of TG are also used to measure elongation (21) and TG synthesis (9, 22). Desaturation flux is measured infrequently, perhaps due to chromatographic considerations (23). Regardless of the species detected, the number of hydrogens available to deuterium exchange is not stoichiometric. Palmitate, for example, has 31 hydrogens but, on average, only 16–22 are labeled by deuterium (24). Thus, experimental mass enrichments are often compared with theoretical values, which vary among lipid species and experimental conditions.

The chemical shift resolution of lipid functional groups by NMR provides discrete positional enrichment that overcomes some challenges of other methods. Incorporation of deuterium into palmitate occurs in a regiospecific fashion (19) through the actions of Fatty acid synthase (FAS) and ELOVL enzymes (**Fig. 1**). One hydrogen derived from water and one from malonyl-CoA are incorporated into each even-numbered carbon of the nascent FA moiety, two hydrogens from NADPH are incorporated into each of the even-numbered carbons of the FA moiety, and three hydrogens from acetyl-CoA are incorporated into the terminal methyl group (25). Thus, methyl enrichment occurs only during DNL, but enrichment in the α1 and α2 hydrogens occurs during DNL and as FAs are elongated (Fig. 1). Because NMR can resolve the proton and deuterium content of these positions, synthesis rates can be determined without assumptions regarding the total number of exchanging hydrogens.

Here, we advance an $^{1}H/^{2}H$ NMR approach (10) to simultaneously examine several classes of FAs, rates of DNL, elongation, desaturation, and glyceride synthesis in an HFD mouse model of obesity and insulin resistance. The method was responsive to genetic and pharmacological gain or loss of function of these pathways. BDF1, a strain of mice susceptible to diet-induced obesity and diabetes (26, 27), developed obesity, massive hyperinsulinemia, mild hyperglycemia, and fatty liver over 35 weeks of an HFD. Hepatic and adipose FA elongation and new TG synthesis were elevated, but DNL was markedly suppressed over several days of ad libitum feeding. Hence, dietary and adipose lipids may contribute more to liver fat than lipogenesis under some conditions in HFD mouse models.

## METHODS

### Animal experiments

Animal protocols were approved by the Institutional Animal Care and Use Committee at the University of Texas Southwestern Medical Center. All mice were male and 12–16 weeks old, except for the HFD experiments (see below). Validation of DNL flux measurement was performed using mice that express a transgenic, constitutively active form of SREBP-1a (n = 5) and littermate controls (n = 5), generated as previously described (28). Validation of desaturase flux detection was performed by oral administration of the SCD-1 inhibitor A939572 (purchased from Biofine) (29, 30). C57BL/6 mice were gavaged with A939572 in DMSO (5 mg/ml) to a total dose of 10 mg/kg (n = 3) or 50 µl of DMSO once at the beginning of the light cycle and once before the end of the light cycle. Validation of elongation flux was performed in C57BL/6 mice (n = 3) gavaged with coconut oil enriched with myristic acid (2 g/10 ml). Coconut oil is rich in medium-chain FAs (12 and 14 carbons) (31, 32). Each animal was gavaged once in the beginning of the light cycle and once in the end of the light cycle with 50 µl/g of the coconut oil mixture and then allowed free access to solid coconut oil in addition to their normal chow. Male BDF1 (cross between female C57BL/6 and male DBA/2) mice (Charles Rivers) (n = 5) were fed either a control semi-synthetic 10% fat diet (Teklad diet TD06416; Harlan Laboratories) or a 60% HFD (Teklad diet

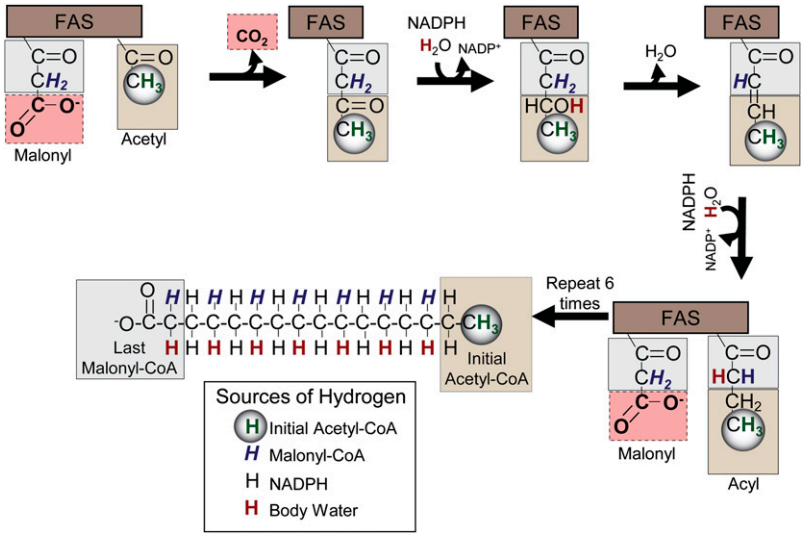


**Fig. 1.** Origin of each hydrogen and carbon in the nascent FA moiety during FA synthesis. FAs are produced from the decarboxylation and condensation of malonyl-CoA with acyl subunits, followed by NADPH-facilitated reduction, dehydration, and a final reduction by NADPH. Each hydrogen in the new palmitate originates from a different source. Hydrogens derived from the initial acetyl-CoA unit (green and circled) are localized in the methyl group of the FA. Even-numbered carbons contain one hydrogen originating from malonyl-CoA (blue and italicized) and one hydrogen originating from body water (red and bold). Both hydrogens bound to odd-number carbons originate from NADPH (black). Carbons originating from the initial acetyl-CoA always occupy the terminal positions (tan box), carbons originating from malonyl-CoA C1 and C2 make up the methylene carbons, and C2 becomes the α2 of the FA during the final elongation step (gray box). The C3 of malonyl-CoA is always lost as $CO_2$ (pink box).

TABLE 1. Contents of mouse diets

| Macronutrients (g/kg) | Control 10% Fat | 60% HFD |
|---|---|---|
| Casein | 210 | 265 |
| Corn starch | 280 | — |
| Maltodextrin | 50 | 160 |
| Sucrose | 325 | 90 |
| Lard | 20 | 310 |
| Soybean oil | 20 | 30 |
| Cellulose | 37 | 65 |

TD06414; Harlan Laboratories) for a period of 35 weeks. For contents of the diets, see **Table 1**.

### $D_2O$ administration and tissue processing

Mice were anesthetized with isoflurane and given a $D_2O$ intraperitoneal injection (27 μl/g) in order to achieve a total body enrichment of ~4%. If mice were treated with an agent by oral gavage, they were injected with $D_2O$ (see below) within 5 min of the last gavage. Mice were then returned to their cages and given ad libitum access to food and 4% $D_2O$ drinking water for a period of 1 to 2 days, except for HFD experiments, which were given 4 days of exposure. Mice were then anesthetized with isoflurane gas, and blood was collected from the hepatic portal vein. Liver and adipose tissue were removed, immediately freeze clamped in liquid nitrogen, and stored at −80°C until further analysis. Tissues were homogenized, and lipids where extracted via Folch extraction (33). Extracts from BDF1 and SREBP-1a Transgenic mice were further purified via silica column solid phase extraction as previously described (34), and the isolated TG fraction was lyophilized and stored at 4°C until further analysis.

### Characterization of coconut oil by MS

The medium-chain composition of coconut oil was confirmed by MS/MS. Coconut oil was diluted 1:2,000 in dichloromethane (DCM)/methanol/isopropyl alcohol (IPA) (1:1:1) with 10 mM ammonium acetate. Solution (300 μl) was injected on the AbSciex 5600 TripleTOF, and data were collected for 5.5 min. TOF data were collected for 1.5 min, and MS/MS of all data were collected for 4 min. The elution solvent was DCM/methanol/IPA (1:1:1). The MS/MS scan rate was 0.16 s for the 200 amu to 1,200 amu range.

### NMR analysis

Lipids were reconstituted in chloroform containing a pyrazine standard (4% $D_5$-pyrazine/ 96% pyrazine, 2 mg/ml). Spectra were obtained at 25°C with a Varian Inova 14.1 T spectrometer equipped with a standard 3 mm broadband probe. Proton NMR spectra were acquired using a 90° pulse, sweep width of 6,000 Hz digitized into 1,300 points, 2 s acquisition time, and 2 s delay (4 s repetition). Spectra were collected with 100 acquisitions (5 min) and were processed by zero filling the free-induction decay to 66,000 points and applying 0.3 Hz of exponential multiplication. Proton-decoupled $^2$H NMR spectra at 92.1 MHz were acquired with a 90° pulse, sweep width of 920 Hz digitized into 1,800 points, resulting in an acquisition time of 2 s A pulse delay of 2 s was used between acquisitions. Spectra were collected for 1 to 24 h and were processed by zero filling the free-induction decay to 8,000 points and applying 0.5 Hz of exponential multiplication. Peak areas were analyzed using the curve-fitting routine supplied with the ACDLabs 1D NMR processor software. Peaks were assigned from literature values (35, 36).

### Lipidomic analysis

*ω-3 FAs.* It is possible to determine the percentage of ω-3 FAs because the terminal methyl group of the ω-3 FAs is slightly downfield of all the other terminal methyl groups (Fig. 3).Therefore, the percentage of ω-3 FAs was determined as follows:

$$\%\ \text{of}\ \omega\text{-3 FAs} = 100 \times \frac{B_{1Ha}}{B_{1Ha} + A_{1Ha}} \qquad \textit{(Eq. 1)}$$

where $B_{1Ha}$ is the $^1$H area of ω-3 FAs, and $A_{1Ha}$ is the $^1$H area of non-ω-3 FAs.

*PUFAs and MUFAs.* The percentage of PUFAs and MUFAs is given by:

$$\%\ \text{PUFA} = 100 \times \frac{(F_{1Ha} + H_{1Ha})}{(2 \times G_{1Ha}) + H_{1Ha}} \qquad \textit{(Eq. 2)}$$

where $F_{1Ha}$ and $H_{1Ha}$ are the $^1$H areas of all PUFAs, $G_{1Ha}$ is the $^1$H area of all FA α2 protons, and $H_{1Ha}$ is the $^1$H area of DHA α2 and α3 protons. Conjugated FAs, whose allylic protons appear between 5 and 6.5 ppm, were not detected in these experiments. However, if conjugated FAs are present in the sample to a high extent, these extra resonances should also be included.

The percentage of MUFAs is given by:

$$\%\ \text{MUFA} = 100 \times \frac{E_{1Ha}}{(2 \times G_{1Ha}) + H_{1Ha}} \qquad \textit{(Eq. 3)}$$

where $E_{1Ha}$ is the $^1$H area of all MUFAs, $G_{1Ha}$ is the $^1$H area of all FA α2 protons, and $H_{1Ha}$ is the $^1$H area of DHA α2 and α3 protons.

The percentage of unsaturated FAs is therefore:

$$\%\ \text{unsaturated FAs} = \%\ \text{PUFAs} + \%\ \text{MUFAs} \qquad \textit{(Eq. 4)}$$

And the amount of saturated FAs is then:

$$\%\ \text{saturated FAs} = 100 - \%\ \text{unsaturated FAs} \qquad \textit{(Eq. 5)}$$

### Calculation of average chain length and molecular weight

In order to calculate average FA chain length, all FAs were considered polymers of a methylenic ($CH_2$) and/or an olefinic (HC = CH) subunit, that is, $^{-}OOC\text{-}(CH_2)_x\text{-}(HC = CH)_y\text{-}CH_3$. Therefore, the average number of protons (ANP) is given by:

$$\text{ANP} = x \times 2 + y \times 2 + 3 \qquad \textit{(Eq. 6)}$$

The average number of carbons (ANC) is given by:

$$\text{ANC} = x + y \times 2 + 2 \qquad \textit{(Eq. 7)}$$

Because all olefinic protons are represented in peak N (Fig. 3), the number of olefinic protons ($y$) is as follows:

$$y = \frac{N_{1Ha}}{2} \qquad \textit{(Eq. 8)}$$

where $N_{1Ha}$ is the $^1$H area of all olefinic protons.

Additionally:

$$\text{ANP} = \frac{\sum_A^K (x_{1Ha})}{\frac{G_{1Ha}}{2} + \frac{H_{1Ha}}{4}} \qquad \textit{(Eq. 9)}$$

where $\sum_{A}^{K}(x_{1Ha})$ is the sum of all corrected areas of peaks arising from the fatty acyl moieties, $G_{1Ha}$ is the $^1$H area of all FA α2 protons, and $H_{1Ha}$ is the $^1$H area of DHA α2 and α3 protons.

Using equations 8 and 9, equation 10 solves for $x$.

$$x = \frac{\sum_{A}^{K}(x_{1Ha})}{\frac{G_{1Ha}}{4} + \frac{H_{1Ha}}{8}} - \frac{N_{1Ha}}{4} - \frac{3}{2} \qquad \textit{(Eq. 10)}$$

where $\sum_{A}^{K}(x_{1Ha})$ is the sum of all corrected areas of peaks arising from the fatty acyl moieties, $N_{1Ha}$ is the $^1$H area of all olefinic protons, $G_{1Ha}$ is the $^1$H area of all FA α2 protons, and $H_{1Ha}$ is the $^1$H area of DHA α2 and α3 protons. The $x$ and $y$ factors calculated in equations 8 and 10 can then be applied in equation 7 to yield the ANC.

These two calculations allow the determination of the average molecular weight (AMW) of the fatty acyl moieties:

$$\begin{aligned}\text{AMW} = {} & \text{ANP} \times 1.008 \\ & + \text{ANC} \times 12.011 + 2 \times 15.999\end{aligned} \qquad \textit{(Eq. 11)}$$

### Linoleic acid and DHA

Linoleic acid (18:2 n-6) and DHA (22:6 n-3) have resolved $^1$H resonances. DHA α2 and α3 protons overlap and appear slightly upfield of the other α2 protons (peak H in Fig. 3). Therefore, the % of DHA is given by:

$$\%\ \text{DHA} = \frac{\frac{H_{1Ha}}{2}}{G_{1Ha} + \frac{H_{1Ha}}{2}} \qquad \textit{(Eq. 12)}$$

where $G_{1Ha}$ is the $^1$H area of all FA α2 protons, and $H_{1Ha}$ is the $^1$H area of DHA α2 and α3 protons.

The bisallylic peaks arising from linoleic acid appear as a clearly defined triplet at ~2.76 ppm (peak J in Fig. 3). Hence, the percentage of linoleic acid is given by:

$$\%\ \text{linoleic acid} = \frac{K_{1Ha}}{G_{1Ha} + \frac{H_{1Ha}}{2}} \qquad \textit{(Eq. 13)}$$

where $K_{1Ha}$ is the $^1$H area of oleic acids bisallylic protons, $G_{1Ha}$ is the $^1$H area of all FA α2 protons, and $H_{1Ha}$ is the $^1$H area of DHA α2 and α3 protons.

### Mass of lipid species present in liver

In order to convert the percentages referred to above into masses, an aliquot of tissue extract was assayed using a commercially available TG detection kit (Sigma, St. Louis, MO). A calibration curve was prepared from various concentrations of triolein. Because the kit detects the TG-glycerol in solution, it is possible to convert the amount of each triolein sample used into its TG-glycerol equivalent, on the basis that the mass ratio of triolein-glycerol is 885.432:92.09. After calculating the amount of TG-glycerol in each sample, the amount of FAs per TG-glycerol is given by:

$$\text{FA/TG glycerol} = \frac{H_{1Ha} + 2 \times G_{1Ha}}{L_{1Ha}} \qquad \textit{(Eq. 14)}$$

where $L_{1Ha}$ is the $^1$H area of TG-glycerol C1 and C3 protons, $G_{1Ha}$ is the $^1$H area of all FA α2 protons, and $H_{1Ha}$ is the $^1$H area of DHA α2 and α3 protons. If a sample contains only TGs, the theoretical value for FA/TG glycerol is 3. If there are FFAs present, the value may be higher, and if diacyl- or monoacyl-glycerols are present, the value may be lower.

The mass (in grams) of TG-FA present in the tissue was calculated by:

$$\text{FA}(\text{g}) = \text{FA/TG glyerol} \times \text{AMW} \times \frac{\text{TG glycerol amount}(\text{g})}{92.09} \qquad \textit{(Eq. 15)}$$

The percentages of species calculated above may then be converted into their respective masses by multiplying the total FA amounts. For example:

$$\text{total linoleic acid}(g) = \text{FA}(g) \times \%\ \text{linoleic acid} \qquad \textit{(Eq. 16)}$$

### Determination of body water enrichment

Body water enrichment was calculated using $^2$H NMR as previously reported (37). Briefly, 10 µl of plasma was added to 190 µl of acetone and a $^2$H NMR spectrum was acquired. Enrichments were calculated by comparing the ratio of the deuterium signal of acetone and water with the previously determined ratios of standards.

### Determination of acetyl-CoA enrichment

In a separate experiment, five male C57BL/6 mice were individually housed and received para-amino benzoic acids (PABAs) to sample hepatic acetyl-CoA and determine its enrichment. $D_2O$ was administered as described above. Drinking water was enriched to 3% and supplemented with 2.5 mg/l of PABA for 3 days to allow the animals to adapt to the compound. One day prior to urine collection the drinking water was replaced with 3% $D_2O$ and 2.5 mg/l PABA (2% PABA-$d_4$). Overnight urine was collected and stored at 4°C until further processing. *N*-acetyl-PABA was purified and processed and analyzed via $^1$H and $^2$H NMR as previously described (38). The total $^2$H enrichment of carbon 2 from the acetyl moiety of *N*-acetyl PABA was calculated by comparing the area of *N*-Ac-PABA $CH_3$ (2.1 ppm) signal with the mean areas of the pair of aromatic PABA-$d_4$ (2.0% $^2$H) signals at 7–8 ppm, which serve as the internal standard.

### Determination of lipid methyl $^2$H enrichment

Peak A represents the methyl hydrogens of non-ω-3 FAs. This signal is corrected for linoleic acid contribution, an essential FA in mammals (39), which does not get labeled with deuterium and would otherwise lead to an underestimation of lipogenic flux. Because the percentage of linoleic acid present in the samples is calculated via equation 13, the corrected methyl enrichment ($A_{eC}$) is given by:

$$A_{eC} = 100 \times \frac{A_{2Ha} \times \%2HS \times P_{1Ha}}{\left(A_{2Ha} \times \%2HS \times P_{1Ha}\right) + \left(A_{1Ha} \times \left[1 - \frac{\%\ \text{linoleic acid}}{100}\right] \times \%1HS \times P_{2Ha}\right)} \qquad \textit{(Eq. 17)}$$

where $A_{1Ha}$ is the $^1$H area of non-ω-3 FAs terminal methyl, $A_{2Ha}$ is the $^2$H area of non-ω-3 FA terminal methyl, $\%2HS$ is the percentage

of deuterium labeled standard (pyrazine), $\%1HS$ is the percentage of deuterium unlabeled standard (pyrazine), $P_{1Ha}$ is the $^1$H area of the pyrazine standard, and $P_{2Ha}$ is the $^2$H area of the pyrazine standard.

In equation 17, and subsequent equations, the proton spectrum is used to normalize the deuterium spectrum (i.e., enrichment); thus, the stoichiometry of the deuterium:proton signals (compared with the pyrazine internal standard) provides an average enrichment of each hydrogen. In effect, the total $^2$H content has been experimentally corrected for the number of protons, obviating the use of a constant.

### DNL

The percentage of FAs formed by DNL during $D_2O$ exposure was calculated as follows:

$$\%\,\mathrm{DNL} = 100 \times \frac{A_{eC}}{\%\ \text{body water enrichment}} \qquad \textit{(Eq. 18)}$$

where $A_{eC}$ is the corrected methyl enrichment calculated above.

The total mass of nonessential FAs is determined as follows:

$$\begin{aligned}\text{Nonessential FAs}&\left(\text{g/g of tissue}\right)\\ &= \text{All FAs}\left(\text{g/g of tissue}\right)\text{-}\omega\text{-3 FAs}\left(\text{g/g of tissue}\right)\\ &- \text{linoleic acid}\left(\text{g/g of tissue}\right)\end{aligned} \qquad \textit{(Eq. 19)}$$

The mass of lipids originating from DNL during $D_2O$ exposure is given by:

$$\mathrm{DNL}\left(\text{g/g of tissue}\right) = \frac{\%\mathrm{DNL}}{100} \times \text{Nonessential FAs}\left(\text{g}\right) \qquad \textit{(Eq. 20)}$$

### FA elongation

The α2 protons are enriched during either DNL or chain elongation. The first pathway involves the complete synthesis of a new FA chain starting from acetyl-CoA, while the second adds acetyl-CoA to preexisting FA chains. Medium chain FAs preexisting the treatment with $D_2O$ will be unlabeled, but if these FAs are elongated during tracer exposure, the subsequently added methylene hydrogens will be labeled. Comparison of the deuterium area at the terminal methyl end of the fatty acyl moieties with that of the α2 protons reports the fractional contribution of elongation to total lipid synthesis:

$$F_{elong} = \left(1 - \frac{A_{2H} \times 2}{H_{2H} \times 3}\right) \qquad \textit{(Eq. 21)}$$

where $A_{2H}$ is the deuterium area of the terminal methyl group of FAs, and $H_{2H}$ is the deuterium area of the α2 protons of FAs. The total percentage of FAs that underwent any degree of elongation can be calculated by the equation:

$$\%\ \text{total elongation} = F_{elong} \times \left(\frac{H_e}{\%\ \text{body water enrichment}}\right) \times 100 \qquad \textit{(Eq. 22)}$$

where $H_e$ is the deuterium enrichment of the α2 hydrogens.

### FA desaturation

Desaturase activity was determined in a similar fashion as lipogenic flux:

$$\%\ \text{Desat.activity} = 100 \times \frac{F_e}{\%\ \text{body water enrichment}} \qquad \textit{(Eq. 23)}$$

where $F_e$ is the deuterium enrichment of the MUFAs' allylic protons.

The total mass of new lipids that were also desaturated during $D_2O$ exposure is given by:

$$\text{Desat. mass}\left(\text{g/g of tissue}\right) = \frac{\%\text{Desat. activity}}{100} \times \text{Unsaturated FAs}\left(\text{g}\right) \qquad \textit{(Eq. 24)}$$

### TG-bound glycerol synthesis

The percentage of newly synthesized glycerol in TG is given by:

$$\%\ \text{glycerol synthesis} = 100 \times \frac{L_e}{\%\ \text{body water enrichment}} \qquad \textit{(Eq. 25)}$$

where $L_e$ is the average deuterium enrichment of the four hydrogens on glycerol C1 and C3.

The mass of newly synthesized glycerol in TG formed during $D_2O$ exposure is given by equation 26. It is important to note that glyceroneogenesis enriches both hydrogens on C1 and C3, glycolysis enriches the two hydrogens on C1 but only one and a half on C3, and glycerol kinase enriches only the two hydrogens on C1 (40). Hence, to the extent that glycolysis and glycerol kinase contribute to glycerol 3-phosphate, TG synthesis could theoretically be underestimated by 12.5% and 50% respectively. However, studies conducted with glycerol tracers have demonstrated rapid equilibration between hepatic glycerol 3-phosphate and the glycolytic/glyceroneogenic pathways prior to esterification, so this underestimation may not be severe (41, 42).

$$\text{new glyceride}\left(\text{g/g tissue}\right) = \frac{\%\ \text{glycerol synthesis}}{100} \times \text{total glyceride} \qquad \textit{(Eq. 26)}$$

$$\text{FA on new triglyceride}\left(\text{g/g tissue}\right) = \frac{\text{new glyceride}}{92} \times 3 \times \text{AMW} \qquad \textit{(Eq. 27)}$$

### Statistical analysis

All data are presented as the mean ± standard error of the mean. Differences between groups were analyzed using an unpaired *t*-test. Differences were considered significant at $P \leqslant 0.05$.

## RESULTS

### Acetyl-CoA enrichment

Analysis of *N*-acetyl-PABA purified from mouse urine was used to determine the acetyl-CoA moiety's enrichment. **Figure 2** shows a typical $^2$H NMR spectra of the purified

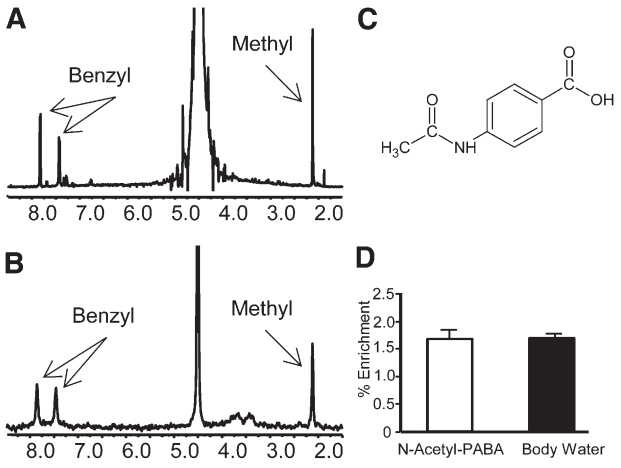


**Fig. 2.** Xenobiotic sampling of liver acetyl-CoA indicates $^{2}H$ enrichment equal to body water. A: $^{1}H$ NMR spectra of *N*-acetyl-PABA. B: $^{2}H$ NMR spectra of *N*-acetyl-PABA. C: *N*-acetyl-PABA molecule. D: Deuterium enrichment in *N*-acetyl-PABA and in body water of mice injected with $D_2O$. Data are presented as the mean ± SE (n = 5).

*N*-Acetyl-PABA. There was no significant difference in the enrichment of *N*-Acetyl-PABA when compared with that of body water (Fig. 2). Therefore, body water was used as a surrogate for acetyl-CoA enrichment in flux calculations.

### Lipid profiles

Mice overexpressing a truncated and constitutively active form of SREBP-1a were first examined to confirm that the NMR methodology accurately detects altered lipid metabolism in vivo. These mice are incapable of downregulating lipogenic genes and therefore have elevated lipid synthesis (28). Saturated FA, MUFA, PUFA, and the special cases of linoleic, ω-6/9, ω-3, and DHA were distinguishable by $^{1}H$ NMR spectra of tissue extracts (**Fig. 3**). SREBP-1a Tg mice had elevated hepatic TG content (supplementary Tables I, II) and a substantially different profile of lipid species than control mice (**Fig. 4A**, **B**). Tg mice had increased percent and total amount of unsaturated FAs, highlighted by an increased MUFA concentration (**Fig. 5A**, **B**). Though still elevated, the increases of essential (linoleic acid), and conditionally essential (ω-3 FAs and DHA) TGs were much less, relative to nonessential FAs.

### Lipogenesis

SREBP-1a transgenic mice had a robust increase in deuterium incorporation into all FA moieties of hepatic TGs compared with controls (Fig. 4C, D and supplementary Table III) with no significant differences in body water enrichment (supplementary Table IV). The increased deuterium incorporation into the methyl position of TG FA translated into a 2-fold increase in percent DNL (Fig. 5C) and a 21-fold increase in the amount of newly synthesized lipids present in the liver of SREBP-1a transgenic mice (Fig. 5D). The fold changes in lipogenesis are similar to values obtained by $^{3}H$ incorporation in these mice (28).

### Glyceride synthesis

Deuterium on glyceride C1 and C3 of TGs was resolved in the $^{2}H$ NMR spectra of tissue extracts (Fig. 3). These positions are enriched when the glycerol 3-phosphate used to esterify FA is synthesized by glyceroneogenesis or glycolysis (40). Inasmuch as glycerol 3-phosphate is enriched before FA esterification, glycerol enrichment indicates TG synthesis (9). The livers of SREBP-1a Tg mice synthesized roughly the same percentage of their glyceride as control mice (Fig. 5E), but the absolute mass of glyceride was elevated 5-fold (Fig. 5F). Essentially all new TGs could be accounted for by DNL in SREBP-1a Tg livers. In contrast, control mice made 3-fold more new TGs than DNL, suggesting that most TGs must have been formed by reesterification of existing FFA (i.e., FFA/TG cycle). Thus, as expected, the fatty liver in SREBP-1a Tg livers was accompanied by a near concomitant increase in TG synthesis.

### Desaturation

In addition to elevated MUFA concentration, SREBP-1a Tg mice had increased deuterium incorporation into monounsaturated olefinic hydrogens (Fig. 4). This finding

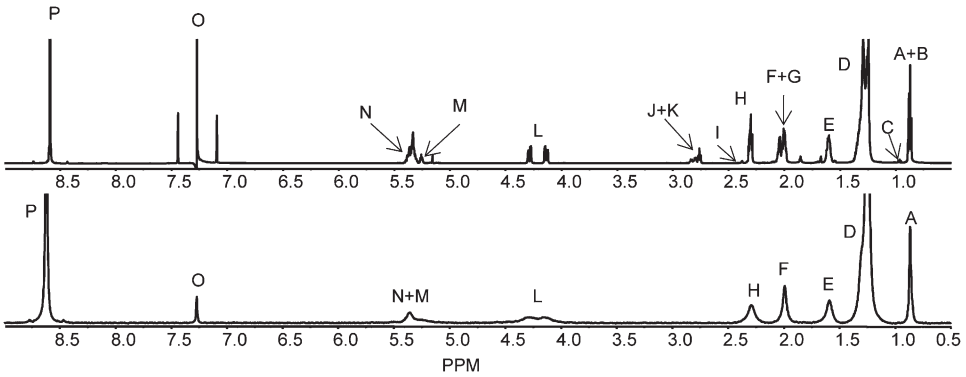


**Fig. 3.** $^{1}H$ (upper) and $^{2}H$ (lower) NMR spectra of a purified TG fraction. Non ω-3 methyl (A); partial ω-6 methyl (B); ω-3 methyl (C); aliphatic chain (D); α3 aliphatic (E); monounsaturated olefinic (F); polyunsaturated olefinic (G); α2 aliphatic (H); DHA α2 and α3 ally (I); linoleic acid bisallylic (J); other bisallylic (K); *sn*-1, *sn*-3 of esterified glycerol (L); *sn*-2 of esterified glycerol (M); olefinic (N); chloroform (O); and pyrazine standard (P).

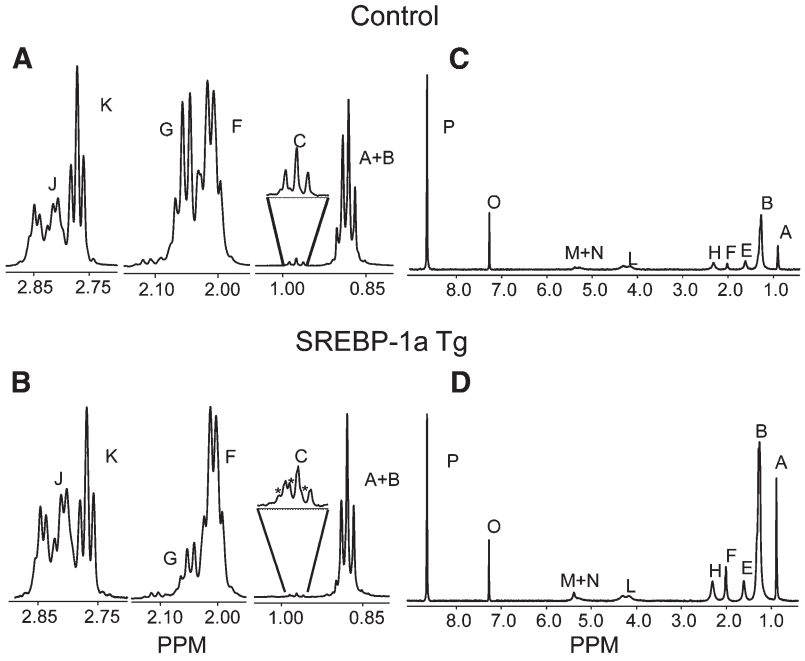


**Fig. 4.** Comparison of key $^{1}$H NMR peaks (A, B) and $^{2}$H NMR spectra (C, D) of the TG moieties of control and SREBP-1a transgenic animals. The peaks marked as * are natural abundance $^{13}$C satellites of peak A. See Fig. 3 for peak assignments.

indicates an ~3-fold increase in the percent of new hepatic lipids undergoing desaturation and an ~40-fold increase in the mass of desaturated lipids formed during $D_2O$ exposure (Fig. 5C, D). This finding is consistent with elevated hepatic SCD-1 expression in these mice (28). To more explicitly confirm the method's ability to detect desaturation flux, we treated WT mice with the SCD-1 inhibitor A939572 (29, 30). Although there was no substantial change in the concentration of unsaturated lipids, deuterium enrichment in olefinic protons was completely suppressed by the inhibitor (**Fig. 6** and supplementary Table III) with no significant differences in body water enrichment (supplementary Table IV), indicating a near absence of SCD-1 activity and desaturation flux.

### Elongation

The α2 hydrogens of the FA TG moieties are labeled with $^{2}$H during the terminal round of chain elongation, while the methyl position is enriched during the initiation of lipogenesis (Fig. 1). Hence, the differences in enrichment at these two sites indicate chain elongation. SREBP-1a Tg livers had a 5-fold increase in the mass of lipids that were elongated during $D_2O$ exposure (Fig. 5D), consistent with the role of SREBP in the positive regulation of elongases (14). To examine whether the NMR method is able to detect more subtle activation of elongation flux, we treated mice with coconut oil containing a 59-fold medium-chain to long-chain FFA ratio and a 1.5-fold medium-chain to long-chain TG-FA ratio (**Fig. 7A**, **B**). Despite a large dose of 12–14 carbon chain length FAs, the chain length of liver TGs was modestly increased from 18 to 18.4 (Fig. 7C). Indeed, deuterium NMR confirmed that the percent contribution of elongation to lipid synthesis was significantly increased in treated mice (Fig. 7D). These findings confirm that $^{2}$H NMR detects changes in elongation in both a robust genetic model and a more subtle substrate model.

### Lipid synthesis in mice on an HFD

To examine the effect of obesity and insulin resistance on lipid synthesis, we studied mice consuming an HFD or matched low-fat diet (LFD) control. The effect of HFD on lipogenesis in C57BL/6 mice has been studied (7–9, 43) previously, so we examined BDF1 mice, a strain suggested to be more susceptible to diet-induced diabetes than the C57BL/6 (26, 27). BDF1 mice on an HFD were significantly heavier than mice on the LFD after week 4 (**Fig. 8A**). Fasting glucose concentration was slightly elevated after 1 week, and fed glucose concentration increased after 14 weeks of the diet (Fig. 8B, C). Both fasting and fed hyperglycemia were most prominent between 16 and 30 weeks. Fasting insulin was significantly elevated after 1 week, and fed insulin was elevated ~30-fold by 25 weeks of HFD (Fig. 8D, E). β-cell dysfunction was previously described in BDF1 mice consuming an HFD (26, 27), but insulin levels continued to rise at 35 weeks when flux experiments were carried out.

As expected, hepatic TG content was increased by 54% in HFD mice compared with controls (**Fig. 9A**, **B**; supplementary Tables V, VI). This elevated TG content occurred with increased polyunsaturated, linoleic acid, DHA, and ω-3 FA composition. Only MUFAs were not increased (Fig. 9A). Changes in the constituents of adipose TG species were less conspicuous, though polyunsaturated and linoleic acids were modestly increased (supplementary Fig. I). To examine the nature of lipid synthesis in obese BDF1 mice, they were given $D_2O$ in drinking water for 4 days prior to analysis of liver and white adipose tissue (WAT) lipid by $^{1}$H/$^{2}$H NMR. An HFD significantly decreased the

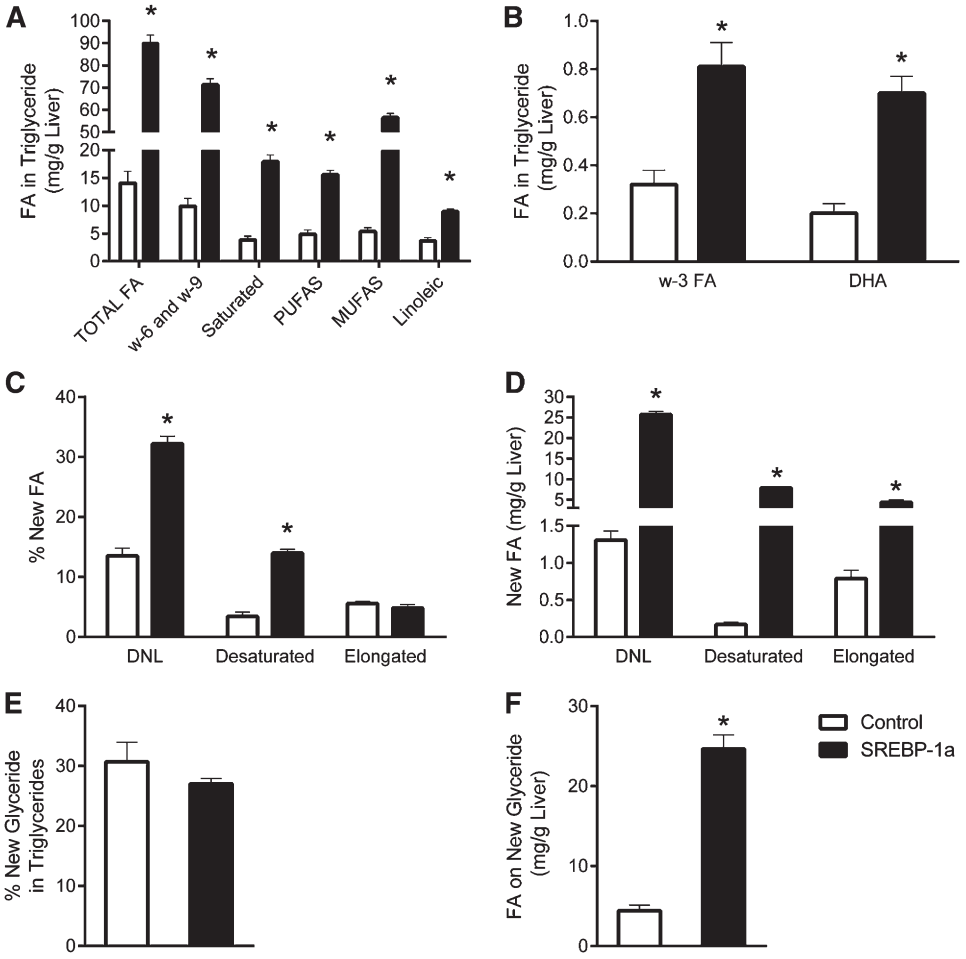


**Fig. 5.** Lipidomic and flux in liver of mice expressing constitutively active SREBP-1a. A, B: Lipid species determined from $^{1}H$ NMR spectra of liver. C: Percent contribution of DNL, desaturation, and elongation to liver TG FAs during 1 day of $^{2}H_2O$ exposure. D: Mass of FAs (attached to TGs) derived from DNL, desaturation, or elongation. E: Percent of TG glycerol that was newly made during $^{2}H_2O$ exposure. F: Mass of FAs on new glyceride. Data are presented as the mean ± SE (n = 5). * Different from control ($P < 0.05$).

deuterium enrichment of FA in hepatic TG (supplementary Table VII) with no significant differences in body water enrichment (supplementary Table VIII). The lower enrichment in the methyl position translated into a decreased percentage (Fig. 9C) and mass (Fig. 9D) of new FAs (i.e., DNL). Newly desaturated FA in liver TG was dramatically decreased by 13-fold (Fig. 9D), consistent with the lack of increased MUFA in HFD livers (Fig. 9A). Similar, but less striking, findings were made in the WAT (supplementary Fig. I). In contrast to DNL and desaturation, chain elongation contributed to 62% of lipid synthesis in HFD mice compared with only 21% in controls. However, because the total amount of lipid synthesis was decreased, there was no difference in the total percentage (Fig. 9C) or mass (Fig. 9D) of lipids derived from elongation.

Roughly 25% of all glyceride in the livers of HFD and control diet mice was made during $D_2O$ exposure (Fig. 9E). Because the amount of TG was elevated in HFD liver, the amount of newly synthesized glycerol in TG was increased (Fig. 9F). Thus, despite a 4-fold lower DNL, glyceride synthesis was increased by 50% and was consistent with the elevated hepatic TG content of HFD mice. These data were even more dramatic in adipose, where the percent of new glyceride was increased by 25% and the mass of new TG was elevated 2-fold (supplementary Fig. I). Taken together, these findings indicate that the HFD suppressed DNL and desaturase flux but did not suppress FA elongation and stimulated TG synthesis in BDF1 mice.

## DISCUSSION

Every odd carbon in a newly synthesized FA receives both of its hydrogens from NADPH, and every even-numbered carbon receives one hydrogen from acetyl-CoA and one from water (Fig. 1). The methyl terminal position is an exception and receives all hydrogens from acetyl-CoA (19). Elongation occurs similar to FA synthesis, with carbon units being added at the carboxyl terminal of the FA. Desaturation occurs without incorporation of new hydrogens. When deuterated water is administered, deuterium enriches these positions proportional to the synthesis rate,

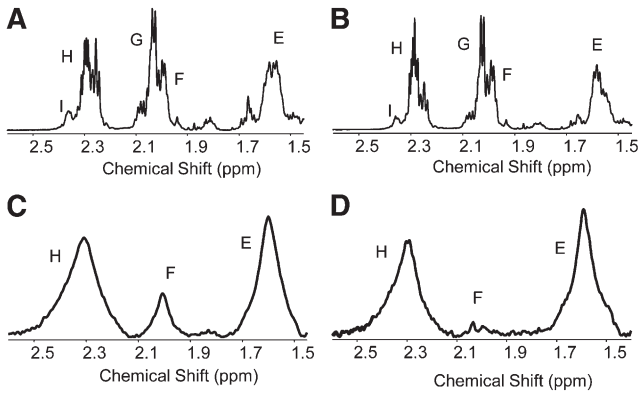


**Fig. 6.** $^{1}$H NMR of hepatic lipids from an animal gavaged with DMSO vehicle (A) or DMSO plus SCD-1 inhibitor (B); $^{2}$H NMR of hepatic lipids from an animal gavaged with DMSO vehicle (C) or DMSO plus SCD-1 inhibitor (D). Animals treated with inhibitor show no deuterium incorporation above natural abundance in their FA olefinic protons (2 ppm), even though the concentration of unsaturated lipid by $^{1}$H NMR is unchanged.

which $^{2}$H NMR detects as stoichiometric peak intensities in the various functional groups of the lipid molecule. Hence, deuterium enrichment in the α2 position represents all lipid synthesis (including elongation), the methyl position represents only DNL, and allylic positions represent new lipids that were also desaturated. Although we focus this study on TGs of the liver and WAT, the methodology is equally applicable to any lipid species (e.g., cholesterol, bile acid, phospholipids) or any tissue that provides enough sample for analysis.

We tested the validity of the approach against model systems with known or predictable perturbations of DNL, desaturation, and elongation. Mice expressing a constitutively active form of SREBP-1a were chosen because they have elevated lipid synthesis across all of these pathways, which were easily detected and consistent with rates reported earlier using $^{3}H_2O$ methods (28). The SCD-1 inhibitor has not been used extensively in vivo but, remarkably, rendered hepatic desaturase activity undetectable, which was consistent with its in vitro efficacy (30). Inhibitors of elongation are not readily available or widely characterized, and genetic interventions were excluded because manipulation of elongase genes has broad effects on lipogenesis and related signaling pathways (14, 43, 44). We chose instead to administer coconut oil/myristic acid, which is abundant in medium-chain FAs. An increase in elongation was observed following coconut oil administration, although somewhat modestly, perhaps, due to the propensity of medium-chain FAs to be oxidized. These results indicate that the methodology is capable of detecting changes in synthesis, desaturation, and elongation of lipids.

Obesity may cause "selective insulin resistance" in liver, such that insulin's suppressive actions on gluconeogenesis are impaired, but its action on SREBP-mediated lipid synthesis is paradoxically maintained (3). This paradox may contribute to NAFLD, so we tested whether flux through pathways of lipid synthesis are altered by HFD-induced obesity and fatty liver in mice. Although, insulin resistance provokes cell signaling (45) and substrate metabolism that generally favors lipogenesis (46), previous tracer studies in lipogenic flux in obese models have produced variable results. Genetically obese rodents have robustly increased lipogenesis (11), but studies in rodents made obese using an HFD have found increased (7), no change (8), and reduced DNL (9–11). To clarify this issue, we examined BDF1 mice fed an HFD because this strain was reported to develop more severe diet-induced diabetes than C57BL/6 mice on a HFD (26, 27). In previous studies, BDF1 mice fed a 64% HFD became insulin resistant by 8 weeks and had fed plasma glucose levels of 335 mg/dl after 14 weeks on the diet (27). Here we found that a 60% HFD caused profound hyperinsulinemia but mild hyperglycemia and was overall consistent with our experience using C57BL/6 mice on this diet (47). The HFD caused fat accumulation in liver, but FA synthesis (i.e., DNL) was markedly decreased. Inasmuch as there is a growing appreciation for the links between insulin resistance, DNL, and fatty liver disease, it is worth discussing some factors that influence studies in lipogenesis during high-fat feeding.

Recent studies measured either total increases in mass isotopes of select lipids following $D_2O$ exposure or the mass isotopomer distribution analysis (MIDA) following $^{13}$C-acetate exposure. Mass isotopomers (M+1, M+2, M+3, and etc.) incorporate into lipids following $D_2O$ administration and can be used to determine new lipid synthesis, assuming the number of exchangeable hydrogens ($n$) on the lipid of interest is known. As reviewed by Previs and colleagues (24), $n$ varies between 16 and 22 for palmitate depending on conditions. Assumptions regarding $n$ are unnecessary for $^{2}$H NMR analysis because the methyl position arises from acetyl-CoA and its enrichment can be measured directly. The assumption that acetyl-CoA enrichment recapitulates body water enrichment applies to both methods and was verified here using a xenobiotic conjugate of acetyl-CoA. Carbon-13 MIDA approaches require another assumption regarding the homogeneity of $^{13}$C-acetate enrichment across the liver sinusoid. All three approaches have been applied to lipogenesis in HFD mice with variable results; MIDA found no change (8), $^{2}$H NMR found a decrease (10), and $^{2}$H mass isotopomers reported both an increase and decrease (7, 9). Although these methods require unique assumptions, differences are likely systematic and hence unlikely related to higher or lower DNL flux in the various HFD studies.

Mass and NMR positional isotopomer analysis place slightly different constraints on the detection of DNL versus chain elongation. Elongation of FAs (C16) to very-long-chain FAs (C18 or longer) occur through ELOVL-mediated chain elongation. An HFD was reported to induce the expression of ELOVL 5 and 6 in one study (48) but suppress their expression in another (12). Using MIDA, Oosterveer and colleagues (8) found that an HFD induced the elongation flux of C16 to C18:1, but not de novo synthesis of C16.

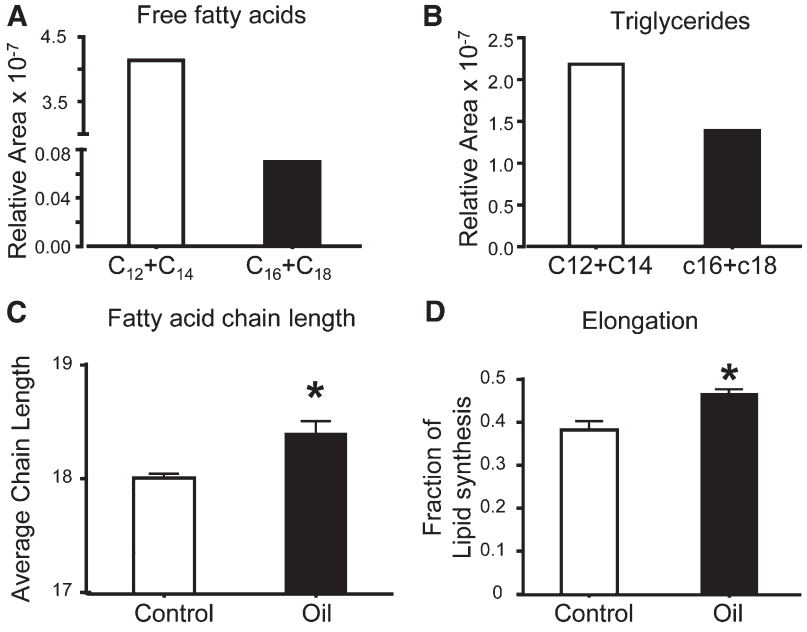


**Fig. 7.** Short and medium chain length composition of FFA (A) and TGs (B) in the coconut oil administered to mice. Hepatic FA chain length (C), and elongation (D) in mice gavaged with vehicle or coconut oil. Data are presented as the mean ± SE (n = 3).

However, if elongation also includes partially catabolized FAs (significantly lower than C16) recycled into the lipogenic pathway (49), it may be detected as DNL by mass isotopomer analysis. NMR positional isotopomer analysis, on the other hand, detects any degree of elongation as enrichment in the α2 but not methyl position. Indeed, mice on the LFD made the vast majority of their new hepatic FAs by DNL, while HFD mice made a slight majority of their lipids by at least one chain elongation. However, the sum of FAs produced by either DNL or at least one elongation was still much lower in HFD mice. Thus, the discrete assignment of lipid synthesis to elongation or DNL is unlikely to account for different findings among the studies.

Experimental HFDs used to induce obesity have a complex influence on lipogenesis (50). A variety of "high-fat" and "control" diet formulations have recently been used in rodent studies in lipogenesis, which could account for a variety of outcomes. Leavens et al. (7) used a hydrogenated coconut oil (58 kcal% or 334 g/kg) diet and found a 2-fold increase in the amount of newly synthesized hepatic lipid. Lard based HFDs produced no change in DNL flux when examined in mice by Oosterveer et al. (8) (344 g/kg for 6 weeks) or a large decrease when studied in rats by Delgado et al. (10) (230 g/kg for 5 weeks) and Lee et al. (11) (120 g/kg for 2 weeks). Lard-based HFDs may override the effects of diet-induced insulin resistance on activation of SREBP-1 (43), while diets containing predominantly saturated fats (e.g., coconut oil) may help induce PPAR-γ coactivator 1β (PGC-1β) coactivation of SREBP-1 and liver X receptor-mediated lipogenesis (51). The type of carbohydrate in experimental diets is another variable that affects lipogenesis. Sucrose is a major carbohydrate source in recent HFD formulations, but not always in the chow used as control diets. We and Brunengraber et al. (9) found reduced DNL in mice consuming a lard-based HFD compared with a matched semisynthetic LFD control containing sucrose. It is possible that the increased sugar in the control diet simply increased lipogenesis compared with the HFD. However, lard-based HFDs suppress lipogenesis even compared with chow diets (10, 11). Nevertheless, the effect of experimental diet-induced obesity on lipogenesis is, at least partially, dependent on the nutrient composition of the diet.

Finally, the timing of tracer exposure may also be critical to the apparent rates of lipogenesis. Two different approaches are common in rodents. One approach administers tracer in the postabsorptive state (e.g., 4–5 h after removal of food) and collects sample before the next feeding period. This acute exposure tests lipogenesis in the postabsorptive state, presumably independent of nutrient absorption and associated substrate or hormonal effects. Using this approach, Leavens and colleagues (7) found that postabsorptive lipogenesis was increased in HFD mice, consistent with selective insulin resistance and constitutive activation of signaling pathways that promote lipogenesis. Another approach measures lipogenesis over 1 or more days of ad libitum feeding. This approach, which was used here, tests the average activity of lipogenesis during feeding and fasting periods. Despite obesity and insulin resistance, lipogenesis was reduced in all cases where HFD rodents were studied across at least one feeding cycle (9–11). In other words, fasting hyperinsulinemia may promote postabsorptive lipogenesis, but during feeding, the dietary fat load likely suppresses lipogenesis. Hence, across meals, liver fat in HFD mice originates from diet or adipose, not DNL.

Despite lower DNL, HFD mice appear to have much greater rates of TG synthesis. Obesity and insulin resistance induce TG synthesis by increasing lipolysis and FFA

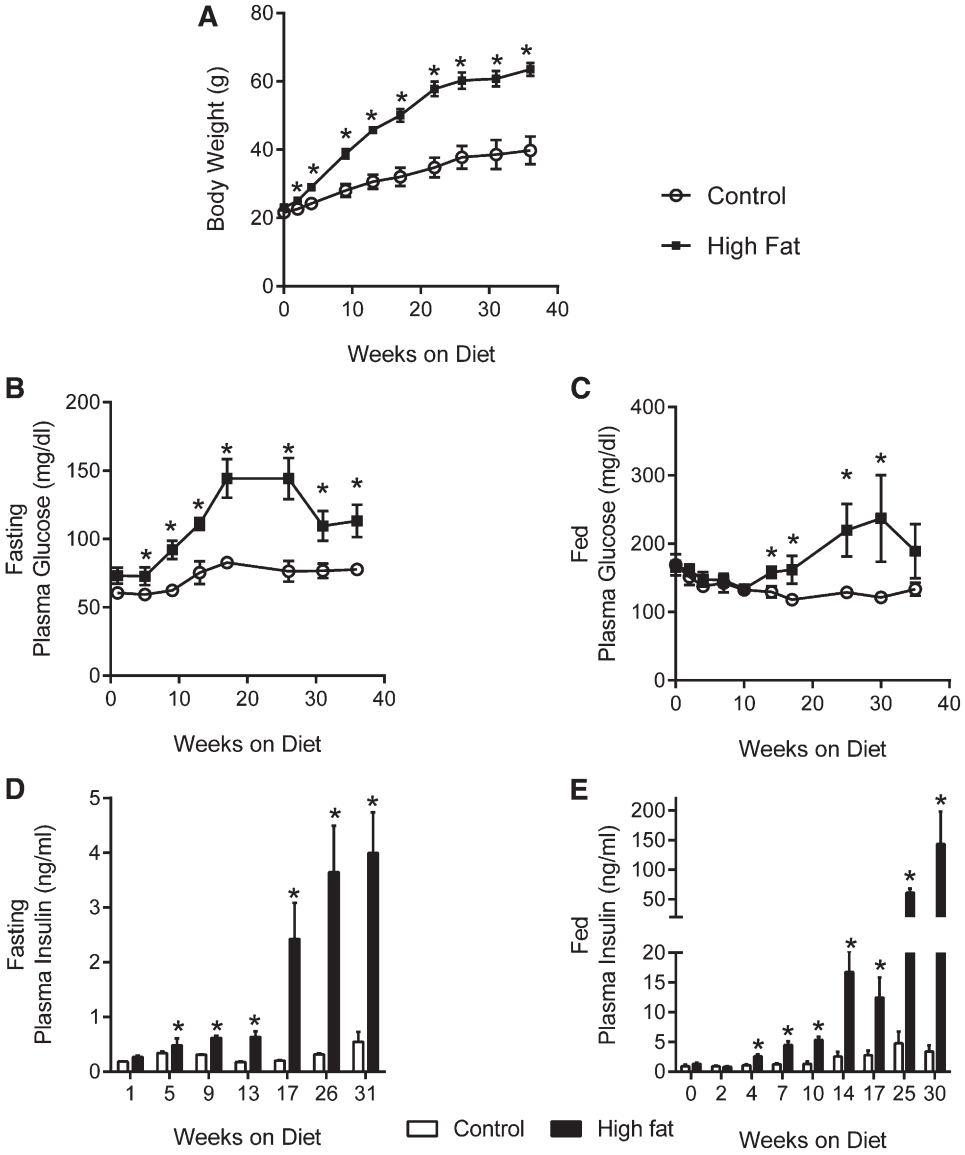


**Fig. 8.** HFD causes obesity and insulin resistance in BDF1 mice. A: Body weight of control and HFD mice. B, C: Fasted and fed plasma glucose. D, E: Fasted and fed plasma insulin. Data are presented as the mean ± SE (n = 4–5).

delivery, much of which is reesterified by the liver. Insulin resistance also increases rates of glyceroneogenesis (52) and provides abundant glycerol-3-phosphate for FFA re/esterification in the glycerol-3-phosphate acyltransferase pathway. Indeed, the mass of FA attached to new glyceride was increased by 50% in liver and 2-fold in adipose of HFD mice. We note that the C1 and C3 enrichment potentially underestimates glyceride synthesis inasmuch as glycerol 3-phosphate is formed directly by the glycerol kinase pathway. However, previous glycerol tracer studies demonstrated that glycerol 3-phosphate equilibrates rapidly with the glycolytic/glyceroneogenic pathway (41, 42), which would minimize the effect. Nevertheless, the data indicate that the liver of mice fed a LFD esterify roughly 2-fold more FA than is made by DNL, while HFD mice esterify >10-fold more FA than is made by DNL. Thus, the vast majority of new hepatic TGs in the liver of HFD mice were formed from the reesterification of existing or ingested lipids.

In summary, we used a novel $^{1}H/^{2}H$ NMR method to investigate lipid synthesis and applied it in mice with HFD-induced insulin resistance. We first confirmed that the method detects altered fluxes by testing it against genetic and pharmacological interventions with known or predictable effects on lipogenesis, desaturation, and/or elongation. An HFD in BDF1 mice caused hyperinsulinemia, increased liver fat, and TG formation but markedly suppressed DNL when examined across feeding periods. Thus, TG synthesis is increased, but the putative increase in lipogenesis and its contribution to liver fat during diet-induced obesity and insulin resistance in mice is less axiomatic than sometimes perceived.

The authors thank Dr. Stephen F. Previs for helpful discussions.

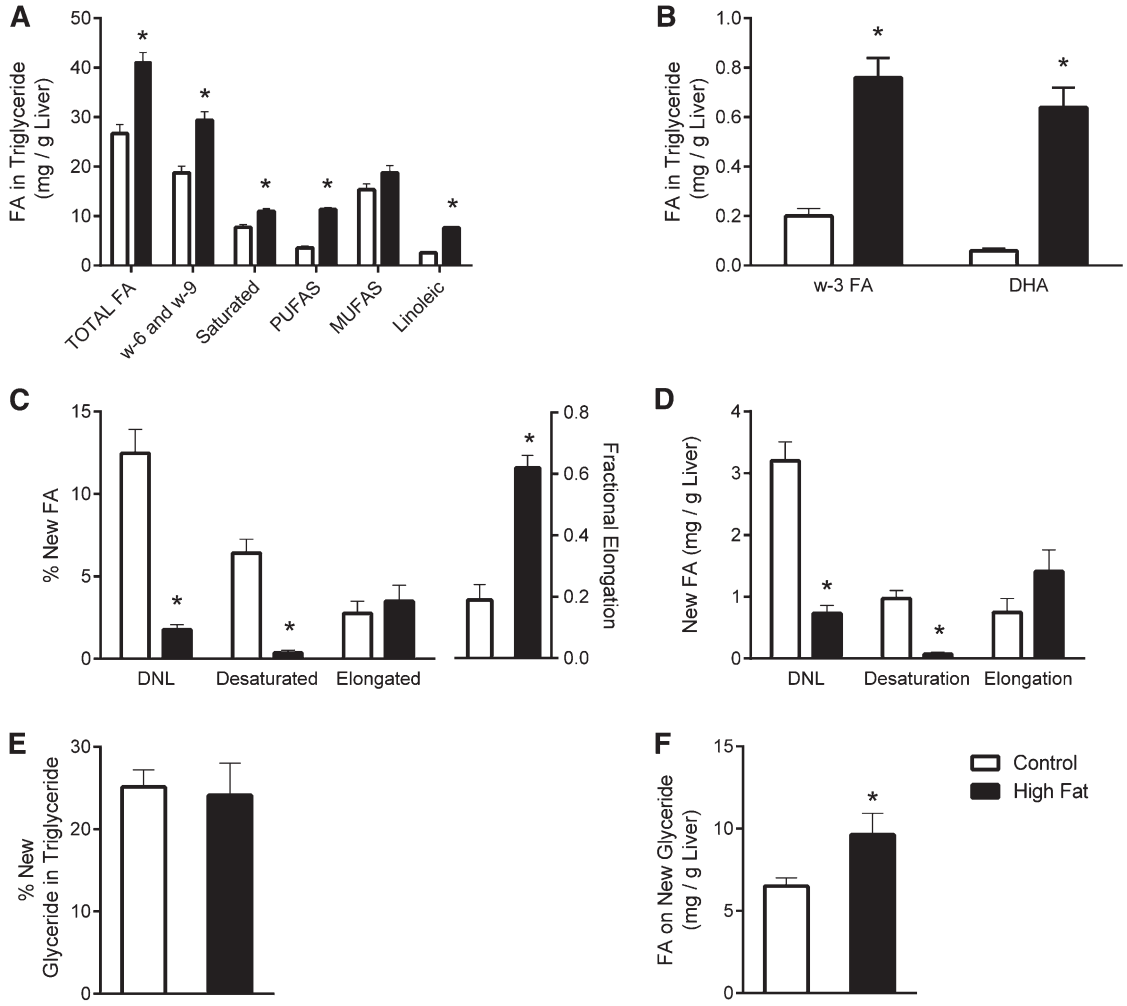


**Fig. 9.** Lipidomic and flux in liver of mice fed an LFD control or HFD. A, B: Lipid species determined from $^{1}$H NMR spectra of liver. C: Percent contribution of DNL, desaturation, and elongation to FAs in liver TG during 4 days of $^{2}H_2O$ exposure. D: Mass of TG FAs derived from DNL, desaturation, or elongation. E: Percent of TG glycerol that was newly made during $^{2}H_2O$ exposure. F: Mass of FAs on new glyceride. Data are presented as the mean ± SE (n = 4–5). * Different from control ($P < 0.05$).

## REFERENCES


1. Glass, C. K., and J. M. Olefsky. 2012. Inflammation and lipid signaling in the etiology of insulin resistance. *Cell Metab.* **15:** 635–645.
2. Muoio, D. M., and C. B. Newgard. 2008. Molecular and metabolic mechanisms of insulin resistance and [beta]-cell failure in type 2 diabetes. *Nat. Rev. Mol. Cell Biol.* **9:** 193–205.
3. Li, S., M. S. Brown, and J. L. Goldstein. 2010. Bifurcation of insulin signaling pathway in rat liver: mTORC1 required for stimulation of lipogenesis, but not inhibition of gluconeogenesis. *Proc. Natl. Acad. Sci. USA.* **107:** 3441–3446.
4. Ricoult, S. J. H., and B. D. Manning. 2013. The multifaceted role of mTORC1 in the control of lipid metabolism. *EMBO Rep.* **14:** 242–251.
5. Lamming, D. W., and D. M. Sabatini. 2013. A central role for mTOR in lipid homeostasis. *Cell Metab.* **18:** 465–469.
6. Lambert, J. E., M. A. Ramos–Roman, J. D. Browning, and E. J. Parks. 2014. Increased de novo lipogenesis is a distinct characteristic of individuals with nonalcoholic fatty liver disease. *Gastroenterology.* **146:** 726–735.
7. Leavens, K. F., R. M. Easton, G. I. Shulman, S. F. Previs, and M. J. Birnbaum. 2009. Akt2 is required for hepatic lipid accumulation in models of insulin resistance. *Cell Metab.* **10:** 405–418.
8. Oosterveer, M. H., T. H. van Dijk, U. J. Tietge, T. Boer, R. Havinga, F. Stellaard, A. K. Groen, F. Kuipers, and D. J. Reijngoud. 2009. High fat feeding induces hepatic fatty acid elongation in mice. *PLoS ONE.* **4:** e6066.
9. Brunengraber, D. Z., B. J. McCabe, T. Kasumov, J. C. Alexander, V. Chandramouli, and S. F. Previs. 2003. Influence of diet on the modeling of adipose tissue triglycerides during growth. *Am. J. Physiol. Endocrinol. Metab.* **285:** E917–E925.
10. Delgado, T. C., D. Pinheiro, M. Caldeira, M. M. Castro, C. F. Geraldes, P. Lopez-Larrubia, S. Cerdan, and J. G. Jones. 2009. Sources of hepatic triglyceride accumulation during high-fat feeding in the healthy rat. *NMR Biomed.* **22:** 310–317.
11. Lee, W. N. P., S. Bassilian, H. O. Ajie, D. A. Schoeller, J. Edmond, E. A. Bergner, and L. O. Byerley. 1994. In-vivo measurement of fatty-acids and cholesterol-synthesis using D2O and mass isotopomer analysis. *Am. J. Physiol. Endocrinol. Metab.* **266:** E699–E708.
12. Wang, Y., D. Botolin, J. Xu, B. Christian, E. Mitchell, B. Jayaprakasam, M. Nair, J. M. Peters, J. Busik, L. K. Olson, et al. 2006. Regulation of hepatic fatty acid elongase and desaturase expression in diabetes and obesity. *J. Lipid Res.* **47:** 2028–2041. [Erratum. 2006. *J. Lipid Res.* 47: 2353.]
13. Jakobsson, A., R. Westerberg, and A. Jacobsson. 2006. Fatty acid elongases in mammals: their regulation and roles in metabolism. *Prog. Lipid Res.* **45:** 237–249.
14. Moon, Y. A., R. E. Hammer, and J. D. Horton. 2009. Deletion of ELOVL5 leads to fatty liver through activation of SREBP-1c in mice. *J. Lipid Res.* **50:** 412–423.
15. Scorletti, E., and C. D. Byrne. 2013. Omega-3 fatty acids, hepatic lipid metabolism, and nonalcoholic fatty liver disease. *Annu. Rev. Nutr.* **33:** 231–248.

16. Liu, X., M. S. Strable, and J. M. Ntambi. 2011. Stearoyl CoA desaturase 1: role in cellular inflammation and stress. *Adv. Nutr.* **2:** 15–22.
17. Matsuzaka, T., A. Atsumi, R. Matsumori, T. Nie, H. Shinozaki, N. Suzuki-Kemuriyama, M. Kuba, Y. Nakagawa, K. Ishii, M. Shimada, et al. 2012. Elovl6 promotes nonalcoholic steatohepatitis. *Hepatology.* **56:** 2199–2208.
18. Fahy, E., S. Subramaniam, R. C. Murphy, M. Nishijima, C. R. Raetz, T. Shimizu, F. Spener, G. van Meer, M. J. Wakelam, and E. A. Dennis. 2009. Update of the LIPID MAPS comprehensive classification system for lipids. *J. Lipid Res.* **50 (Suppl.):** S9–S14.
19. Murphy, E. J. 2006. Stable isotope methods for the in vivo measurement of lipogenesis and triglyceride metabolism. *J. Anim. Sci.* **84 (Suppl.):** E94–E104.
20. Diraison, F., C. Pachiaudi, and M. Beylot. 1997. Measuring lipogenesis and cholesterol synthesis in humans with deuterated water: use of simple gas chromatographic mass spectrometric techniques. *J. Mass Spectrom.* **32:** 81–86.
21. Lee, W. N., S. Bassilian, S. Lim, and L. G. Boros. 2000. Loss of regulation of lipogenesis in the Zucker diabetic (ZDF) rat. *Am. J. Physiol. Endocrinol. Metab.* **279:** E425–E432.
22. Bederman, I. R., S. Foy, V. Chandramouli, J. C. Alexander, and S. F. Previs. 2009. Triglyceride synthesis in epididymal adipose tissue contribution of glucose and non-glucose carbon sources. *J. Biol. Chem.* **284:** 6101–6108.
23. Castro-Perez, J. M., T. P. Roddy, V. Shah, D. G. McLaren, S. P. Wang, K. Jensen, R. J. Vreeken, T. Hankemeier, D. G. Johns, S. F. Previs, et al. 2011. Identifying static and kinetic lipid phenotypes by high resolution UPLC-MS: unraveling diet-induced changes in lipid homeostasis by coupling metabolomics and fluxomics. *J. Proteome Res.* **10:** 4281–4290.
24. Previs, S. F., A. Mahsut, A. Kulick, K. Dunn, G. Andrews-Kelly, C. Johnson, G. Bhat, K. Herath, P. L. Miller, S-P. Wang, et al. 2011. Quantifying cholesterol synthesis in vivo using 2H2O: enabling back-to-back studies in the same subject. *J. Lipid Res.* **52:** 1420–1428.
25. Jungas, R. L. 1968. Fatty acid synthesis in adipose tissue incubated in tritiated water. *Biochemistry.* **7:** 3708–3717.
26. Hull, R. L., K. Kodama, K. M. Utzschneider, D. B. Carr, R. L. Prigeon, and S. E. Kahn. 2005. Dietary-fat-induced obesity in mice results in beta cell hyperplasia but not increased insulin release: evidence for specificity of impaired beta cell adaptation. *Diabetologia.* **48:** 1350–1358.
27. Karasawa, H., S. Nagata-Goto, K. Takaishi, and Y. Kumagae. 2009. A novel model of type 2 diabetes mellitus based on obesity induced by high-fat diet in BDF1 mice. *Metabolism.* **58:** 296–303.
28. Shimano, H., J. D. Horton, R. E. Hammer, I. Shimomura, M. S. Brown, and J. L. Goldstein. 1996. Overproduction of cholesterol and fatty acids causes massive liver enlargement in transgenic mice expressing truncated SREBP-1a. *J. Clin. Invest.* **98:** 1575–1584.
29. Xin, Z., H. Zhao, M. D. Serby, B. Liu, M. Liu, B. G. Szczepankiewicz, L. T. Nelson, H. T. Smith, T. S. Suhar, R. S. Janis, et al. 2008. Discovery of piperidine-aryl urea-based stearoyl-CoA desaturase 1 inhibitors. *Bioorg. Med. Chem. Lett.* **18:** 4298–4302.
30. von Roemeling, C. A., L. A. Marlow, J. J. Wei, S. J. Cooper, T. R. Caulfield, K. Wu, W. W. Tan, H. W. Tun, and J. A. Copland. 2013. Stearoyl-CoA desaturase 1 is a novel molecular therapeutic target for clear cell renal cell carcinoma. *Clin. Cancer Res.* **19:** 2368–2380.
31. Rioux, V., P. Lemarchal, and P. Legrand. 2000. Myristic acid, unlike palmitic acid, is rapidly metabolized in cultured rat hepatocytes. *J. Nutr. Biochem.* **11:** 198–207.
32. Rioux, V., S. Daval, H. Guillou, S. Jan, and P. Legrand. 2003. Although it is rapidly metabolized in cultured rat hepatocytes, lauric acid is used for protein acylation. *Reprod. Nutr. Dev.* **43:** 419–430.
33. Folch, J., M. Lees, and G. H. Sloane Stanley. 1957. A simple method for the isolation and purification of total lipides from animal tissues. *J. Biol. Chem.* **226:** 497–509.
34. Hamilton, J. G., and K. Comai. 1988. Rapid separation of neutral lipids, free fatty acids and polar lipids using prepacked silica Sep-Pak columns. *Lipids.* **23:** 1146–1149.
35. Willker, W., and D. Leibfritz. 1998. Assignment of mono- and polyunsaturated fatty acids in lipids of tissues and body fluids. *Magn. Reson. Chem.* **36:** S79–S84.
36. Siddiqui, N., J. Sim, C. J. Silwood, H. Toms, R. A. Iles, and M. Grootveld. 2003. Multicomponent analysis of encapsulated marine oil supplements using high-resolution 1H and 13C NMR techniques. *J. Lipid Res.* **44:** 2406–2427.
37. Jones, J. G., M. Merritt, and C. Malloy. 2001. Quantifying tracer levels of (2)H(2)O enrichment from microliter amounts of plasma and urine by (2)H NMR. *Magn. Reson. Med.* **45:** 156–158.
38. Carvalho, F., J. Duarte, A. R. Simoes, P. F. Cruz, and J. G. Jones. 2013. Noninvasive measurement of murine hepatic acetyl-CoA 13C-enrichment following overnight feeding with 13C-enriched fructose and glucose. *Biomed. Res. Int.* **2013:** 638085.
39. Burr, G. O., M. M. Burr, and E. S. Miller. 1932. On the fatty acids essential in nutrition. III. *J. Biol. Chem.* **97:** 1–9.
40. Chen, J. L., E. Peacock, W. Samady, S. M. Turner, R. A. Neese, M. K. Hellerstein, and E. J. Murphy. 2005. Physiologic and pharmacologic factors influencing glyceroneogenic contribution to triacylglyceride glycerol measured by mass isotopomer distribution analysis. *J. Biol. Chem.* **280:** 25396–25402.
41. Patterson, B. W., B. Mittendorfer, N. Elias, R. Satyanarayana, and S. Klein. 2002. Use of stable isotopically labeled tracers to measure very low density lipoprotein-triglyceride turnover. *J. Lipid Res.* **43:** 223–233.
42. Previs, S. F., C. A. Fernandez, D. Yang, M. V. Soloviev, F. David, and H. Brunengraber. 1995. Limitations of the mass isotopomer distribution analysis of glucose to study gluconeogenesis: substrate cycling between glycerol and triose phosphates in liver. *J. Biol. Chem.* **270:** 19806–19815.
43. Tripathy, S., M. Torres-Gonzalez, and D. B. Jump. 2010. Elevated hepatic fatty acid elongase-5 activity corrects dietary fat-induced hyperglycemia in obese C57BL/6J mice. *J. Lipid Res.* **51:** 2642–2654.
44. Tripathy, S., and D. B. Jump. 2013. Elovl5 regulates the mTORC2-Akt-FOXO1 pathway by controlling hepatic cis-vaccenic acid synthesis in diet-induced obese mice. *J. Lipid Res.* **54:** 71–84.
45. Leavens, K. F., and M. J. Birnbaum. 2011. Insulin signaling to hepatic lipid metabolism in health and disease. *Crit. Rev. Biochem. Mol. Biol.* **46:** 200–215.
46. Otero, Y. F., J. M. Stafford, and O. P. McGuinness. 2014. Pathway-selective insulin resistance and metabolic disease: the importance of nutrient flux. *J. Biol. Chem.* **289:** 20462–20469.
47. Satapati, S., N. E. Sunny, B. Kucejova, X. Fu, T. T. He, A. Mendez-Lucas, J. M. Shelton, J. C. Perales, J. D. Browning, and S. C. Burgess. 2012. Elevated TCA cycle function in the pathology of diet-induced hepatic insulin resistance and fatty liver. *J. Lipid Res.* **53:** 1080–1092.
48. Kozawa, S., A. Honda, N. Kajiwara, Y. Takemoto, T. Nagase, H. Nikami, Y. Okano, S. Nakashima, and N. Shimozawa. 2011. Induction of peroxisomal lipid metabolism in mice fed a high-fat diet. *Mol. Med. Rep.* **4:** 1157–1162.
49. Abu-Elheiga, L., H. Wu, Z. Gu, R. Bressler, and S. J. Wakil. 2012. Acetyl-CoA carboxylase 2−/− mutant mice are protected against fatty liver under high-fat, high-carbohydrate dietary and de novo lipogenic conditions. *J. Biol. Chem.* **287:** 12578–12588.
50. Strable, M. S., and J. M. Ntambi. 2010. Genetic control of de novo lipogenesis: role in diet-induced obesity. *Crit. Rev. Biochem. Mol. Biol.* **45:** 199–214.
51. Lin, J., R. Yang, P. T. Tarr, P-H. Wu, C. Handschin, S. Li, W. Yang, L. Pei, M. Uldry, P. Tontonoz, et al. 2005. Hyperlipidemic effects of dietary saturated fats mediated through PGC-1β coactivation of SREBP. *Cell.* **120:** 261–273.
52. Millward, C. A., D. DeSantis, C-W. Hsieh, J. D. Heaney, S. Pisano, Y. Olswang, L. Reshef, M. Beidelschies, M. Puchowicz, and C. M. Croniger. 2010. Phosphoenolpyruvate carboxykinase (Pck1) helps regulate the triglyceride/fatty acid cycle and development of insulin resistance in mice. *J. Lipid Res.* **51:** 1452–1463.